LBL-8419

CONF-781029--1

Presented at the International Symposium on Factors in Densification and Sintering of Oxide and Non-Oxide Ceramics, Hakone, Japan, October 3-6, 1978

THERMODYNAMICS AND MECHANISMS OF SINTERING

Joseph A. Pask

October 1978

Prepared for the U. S. Department of Energy
under Contract W-7405-ENG-48

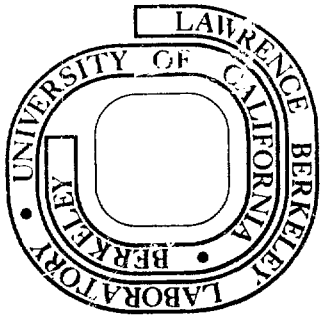

change of the integrated surface free energy (negative) plus the change of the integrated grain boundary energy (positive). When the sum is negative the densification process proceeds.[1,2] In real systems the specific free energies, γ_{SV} and γ_{GB}, would have several values because of their anisotropic nature or dependence on crystallographic orientations.

MODEL SYSTEMS

The first hypothetical step is the analysis of the sintering of two spheres with assumed isotropic interfacial energies. A grain boundary must form which grows as the centers of the spheres move toward each other by an amount indicated as h in Fig. 1. With occurrence of this shrinkage the most logical path for mass transport is along the grain boundary to the neck and from the neck to the free surfaces of the spheres. This amounts to a two-step process.[3] When the second step is faster, the spherical shape of the free surfaces is maintained and the dihedral angle formed along a plane passing through the centers of the spheres, as shown in the upper sketch of Fig. 1, increases with shrinkage. When dG becomes zero, the equilibrium angle is reached; further shrinkage does not occur because a positive change in dG would occur due to the second term becoming larger than the first. The following equation holds:

$$dG = \gamma_{SV} dA_{SV} + \gamma_{GB} dA_{GB}. \qquad (2)$$

This configuration then constitutes metastable equilibrium for the system with an equilibrium dihedral angle. It should also be noted that the grain boundary can not move in this configuration because any movement would cause an increase of grain boundary area which would not be possible thermodynamically. When the first step is faster, a neck forms with an

equilibrium dihedral angle. The neck surface, however, exhibits reverse curvature in planes passing through the centers of the spheres, as shown in lower sketch of Fig. 1. As mass transport occurs from the neck to the free surfaces during the second step upsetting the equilibrium dihedral angle, the faster first step brings the angle back to equilibrium causing shrinkage. As this process continues, the reverse curvature keeps decreasing until the top configuration and equilibrium are reached.

The next step is an analysis of the specific driving forces for mass transport. These are due to the presence of reverse curvature in free surfaces and nonequilibrium dihedral angles. Figure 2 indicates a cross-section through a neck region in the early stages of sintering when reverse curvature exists, illustrated by points 3 and 4 in the sketch; the dihedral angle is Φ. The γ_{GB} is actually the sum of $\gamma_{S_2S_1}$ and $\gamma_{S_1S_2}$ which in the model system are equal but in most real systems are not equal. Then, it can be seen that $\gamma_{S_2S_1} < \gamma_{S_2V}$ and $\gamma_{S_1S_2} < \gamma_{S_1V}$ and that

$$\gamma_{GB} = \gamma_{S_1V}\cos\Phi/2 + \gamma_{S_2V}\cos\Phi/2 = 2\gamma_{SV}\cos\Phi/2. \qquad (3)$$

The maximum value for γ_{GB}/γ_{SV} becomes 2 when Φ is equal to zero. The chemical potentials for vacancies, and thus the vacancy concentrations, would follow the following sequence at non-equilibrium:

$$\mu_4 > \mu_3 > \mu_2 > \mu_1 \geq \mu_B \qquad (4)$$

With an equilibrium dihedral angle, $\mu_1 = \mu_2 = \mu_3$.

In the presence of reverse curvature $\mu_4 > \mu_3$; the flow of vacancies is from site 4 to site 3 and atoms to site 4, probably by bulk diffusion in the

near-surface region. This causes μ_3 to become greater than μ_2; matter then moves from site 2 to site 3 followed by movement from site 1 to site 2 causing the centers of the spheres to move towards each other. In the absence of reverse curvature and an equilibrium dihedral angle (Fig. 1a), $\mu_1 = \mu_2 = \mu_3$ which does not become upset.

The next step is an analysis of the sintering of a pore formed by 3 spheres in a (111) plane in fcc packing.[1] It can be seen in Fig. 3 that as grain boundaries form at contact points and assuming that step 2 is faster than step 1 in mass transport, the dihedral angle increases from zero degrees and when the pore closes, Φ is approaching 60° which corresponds to a γ_{GB}/γ_{SV} of 1.734. The same pattern would hold if necks formed at the grain boundaries (step 1 faster than step 2), just as discussed for the 2-sphere model. Figure 4 shows fcc packing of spheres (0.26 fractional void volume) along the (100), (111) and (110) planes without shrinkage in row A. Interpenetration and grain boundary formation continues until pores on the (111) plane close, as described in Fig. 3, which is represented by row B; at this point the fractional void volume is 0.035, and the fractional linear shrinkage is 0.084. Continued shrinkage until the pores along (100) planes close is represented by row C; this requires a size reduction of the (111) plane which complicates the mass diffusion path. Continuing shrinkage results in the closing of the pores on the (110) planes and complete densification; at this point the fractional linear shrinkage is 0.095 and Φ is 109° ($\gamma_{GB}/\gamma_{SV} = 1.161$). In this model system the sintering process consists of an initial (open pore with no grain growth) stage and a final (closed pore with potential grain growth) stage; no intermediate stage represented by grain growth

and the presence of open pores exists. It should be noted that if the material system had a ratio of γ_{GB}/γ_{SV} less than 1.161, no thermodynamic barrier for complete densification would exist; a value greater than 1.161 would indicate that equilibrium dihedral angles would be reached before the system had completely densified resulting in an end point density.

The next step is to analyze the sintering of a planar pore formed by four spheres in a (100) plane in sc packing (0.48 fractional void volume). As grain boundaries grow at contact points (Fig. 5) and assuming that step 2 is faster than step 1, the dihedral angle increases and when the pore closes, Φ is approaching 90° which corresponds to a γ_{GB}/γ_{SV} of 1.416. When these planar pores close, closed pores are present since the (110) planes are not completely densified, as seen in Fig. 6; at this point the fractional linear shrinkage is 0.184. Continued shrinkage results in complete densification with a linear shrinkage of 0.196 for which a γ_{GB}/γ_{SV} ratio smaller than 1.161 is required. As in the fcc system, the sintering process would consist only of initial and final stages It should be observed that the maximum γ_{GB}/γ_{SV} ratio permissable to form closed pores decreases with less dense packings of spheres. This point is further illustrated by the densification of a model system with diamond cubic (dc) packing (0.68 fractional void volume). The open packing with a small coordination number of spheres around a sphere is represented in Fig. 7. In this case closed pores form (end of initial stage) with Φ at 105° which is equivalent to a γ_{GB}/γ_{SV} ratio of 1.226; the fractional void volume then is 0.101 and the linear shrinkage, 0.277. Complete densification requires a γ_{GB}/γ_{SV} ratio of

1.074 and indicates a shrinkage of 0.316.

The next step is to analyze the effect of the nature of regular packing of uniform size spherical grains on shrinkage. Figure 8 indicates three types of regular packings which represent fcc, sc and dc packings, and the hypothetical decrease in porosity vs. time curves. The amount of interpenetration at every contact in a given time at a given temperature regardless of the type of packing is the same until closed pores are formed in the most dense or fcc packing. The densification curves under these ideal model conditions are directly proportional to time and coincide until the fcc packing closed pores form; the straight line continues until closed pores form in the sc packing; and so on. It is seen that the basic difference in the curves is only in the amount of shrinkage that has to be realized for a given packing before closed pores form; this portion represents the initial stage. The closed pore or final stage does not follow this linear relationship of porosity vs. time. It can be seen that the amount of linear shrinkage per unit length in a given time would also be the same for all packings before any closed pores form.

The next step is to explore the effect of sphere size on densification rates. Illustrative schematics are shown in Fig. 9 which are based on sc packing of spherical grains. The number of contacts in a unit length doubles for every decrease of diameter of the spheres by half; this exponential increase is shown in the upper left plot. Since shrinkage occurs at every contact point, the amount of shrinkage and the amount of decrease of porosity in a given time likewise increases with decrease of grain size. The total shrinkage and the two stages of

sintering, however, remain constant regardless of grain size if the packing is the same, except for the time parameter. These points are illustrated by the upper right plot. Extremely fine particles, thus, can be considered to be reactive in comparison with coarser grain compacts just on the basis of particle size.

The next step is to consider the importance of homogeneity in efforts to reach theoretical density. Figure 10 represents an initial close-packed plane which was sintered to complete densification to form a hexagonal network of grain boundaries except for a pore on a grain boundary which formed because of some irregularity at that point, and an absent grain whose site became a pore. Although the small pore fulfills the requirement of being on a triple point, it will not decrease in size since it is isolated and thus the whole compact would have to decrease by an equivalent volume which is kinetically too slow. On the other hand, if equivalent small pores were present on every triple point, or uniformly distributed on the triple points, then there would be relatively short diffusion paths between pores and each pore would shrink cooperatively to realize theoretical density (assuming that the γ_{GB}/γ_{SV} ratio for these grains was less than 1.734 since this packing represented a close-packed plane in fcc configuration). The large pore formed by an absent grain indicates an equilibrium configuration with equilibrium dihedral angles; it would thus be stable. A large pore with many grains coordinating it was formed in an alumina compact that had organic spheres added during mixing which were oxidized on firing. It is shown in Fig. 11. The equilibrium configuration of the dihedral angles can be seen. This pore will not shrink because there is no specific driving force for

mass transport.

REAL SYSTEMS

It is thus evident that in hypothetical model systems no grain growth, which requires grain boundary motion, can occur. In real systems, however, grain growth does occur at some time during the initial stage, i.e. while open pores are still present, which corresponds to the initiation of the intermediate stage of sintering. Grain growth readily occurs during the final stage.

The question then arises as to why grain boundaries move and thus grain growth occurs. The responsible factors for grain growth in real systems are (a) the presence of a range of grain and particle sizes and shapes, (b) anisotropy of surface and grain boundary energies, and (c) non-homogeneity due to aggregation, agglomeration and non-uniformity in packing. Some examples of effects due to such irregularities are illustrated in Fig. 12. The top series of sketches illustrate the interpenetration of a large and small sphere. The grain boundary becomes curved because of the influence and requirements of the dihedral angle position due to the greater interpenetration of the smaller sphere in a given time; this fact plus the relatively early growth of the grain boundary to be approximately equal to the diameter of the small sphere creates a situation which makes movement of the grain boundary out of a small grain thermodynamically feasible.

It is an accepted fact that a curved grain boundary can move towards its center of curvature. Such a movement is thermodynamically acceptable since its area is reduced in the process. It can be shown, however, that even a straight boundary can move because of the presence of anisotropy

in interfacial energies. In Fig. 12, for instance, two grains are shown forming a grain boundary whose energy is the sum of $\gamma_{S_2S_1}$ and $\gamma_{S_1S_2}$. On the basis of the indicated structures it can be postulated that $\gamma_{S_1S_2} > \gamma_{S_2S_1}$; therefore, the μ and the vacancy concentration in S_1 at the grain boundary is greater than in S_2. The grain boundary could then move into grain 2. There could, however, be a reorientation of the grain boundary as well so that $\gamma_{S_1S_2}$ becomes equal to $\gamma_{S_2S_1}$ as shown in the second sketch; in this position no further movement occurs because of loss of anisotropy and the associated thermodynamic driving force. In a real system with anisotropy of surface energies and various grain and particle shapes the potential of some anisotropy and nonsymmetrical dihedral angles with associated potential grain boundary motion exists at every contact point. Such details have not as yet been worked out.

The last sketch in Fig. 12 shows a pore on a curved grain boundary.[1] It can be shown energetically that an isotropic grain boundary can not break away from the pore unless a sufficient curvature exists in the grain boundary in order to have a reduction in the free energy of the system as the grain boundary straightened out. Such events lead to entrapped pores within the grains which literally are impossible to eliminate by diffusion because the entire grain would have to shrink in size causing difficulties of maintaining contiguity at grain boundaries.

Another factor that causes problems in the presence of agglomerated or aggregated particles in the powder because they are the source of inhomogeneities. If the particles are more densely packed than the matrix or if they are an assembly of fine particles, according to Figs. 8 and 9 they would densify earlier becoming the focus for exaggerated grain

growth. On the other hand, if the particles are less densely packed than the matrix, the matrix densifies first and the particle regio retain a porous structure which can not be eliminated. On the other hand, many kinetic analyses are based on a change in pore size and shape; these changes are also dependent on the factors that affect grain growth variations. Another factor, whose effect can be most easily followed by pore changes, is aggregation during sintering because of inhomogeneities in packing of powders and failure to form grain boundaries at all initial contact points.

SUMMARY DISCUSSION

Analyses of model and real systems indicate that the most critical factors in realizing uniform microstructures are homogeneity and uniformity of packing in the powder compact. If agglomerates and aggregates are present, processing procedures should be devised that would prevent their formation or, if they form, break them down either in the powder processing or fabrication steps.

The starting powders should consist of small and uniform grains since they then are "reactive" on the basis of providing many more grain-grain contacts. If a microstructure with small grains is desired, a starting powder with small and uniform-sized grains is necessary. Furthermore, since grain growth is dependent on grain boundary motion which in turn is largely due to the anisotropy of structures and interfacial energies, any additives that would reduce this anisotropy would be desirable.

Although there is no unique value of γ_{GB}/γ_{SV} in a real system because of the anisotropy of interfacial energies, it does not exclude the

requirement that the values for this ratio should be as small as possible. Theoretically, the smaller the % theoretical density of the powder compacts, the smaller the γ_{GB}/γ_{SV} ratios should be to realize theoretical density in the sintered compacts. If the ratio is too large, a thermodynamic end point density may be the result. Any additive that would reduce the γ_{GB}/γ_{SV} values is thus desirable.

It is also worthwhile to summarize the sintering mechanisms as presently deduced from these model analyses. Firstly, in densifying systems the mass transport must occur in two steps: movement from grain boundaries formed by contacts to the neck region, and from the neck region to the free surfaces. In most real systems a neck forms and the slow step in sintering is the movement of material in the neck region to the free surface regions due to a thermodynamic driving force of reverse curvature in the free surfaces. In special cases, a steady state neck does not form and the slow step is movement of material in the grain boundaries to the neck region due to a thermodynamic specific driving force of the presence of nonequilibrium dihedral angle formed at the contact grain boundary. These special cases are represented by conditions which favor removal of material from the neck region as it moves into the neck and redistributing it. (Examples are sintering of MgO compacts in water vapor atmosphere,[4] and liquid phase sintering).

Secondly, an identification of the stages of sintering would be in order since their identification in literature has not been consistent. The events that occur in the process of establishing real contacts and a steady state framework structure have been identified here as the PRELIMINARY STAGE which includes any rearrangement of the grains or

particles and formation of necks. This terminology was chosen since some systems may not have any preliminary stage events and the formation of necks may involve contributions of several mechanisms. The INITIAL STAGE corresponds to the period when shrinkage occurs with decreasing pore sizes but with no grain growth and no formation of closed pores. The FINAL STAGE of sintering corresponds to the period when no open pores are present. Grain growth can occur during this period and can also continue into an annealing period after the system has reached its maximum density, but not necessarily theoretical density. In real systems, because of a range of particle sizes and shapes and anisotropy of interfacial energies, grain growth starts at some point in the initial stage which then constitutes the beginning of the INTERMEDIATE STAGE. An example of the effect of an intermediate stage on the kinetics is illustrated by the dash-curve in Fig. 9. Closed pores are progressively formed during this stage, but the final stage does not start until all open pores become closed. Inspection then indicates that the length of the intermediate stage is variable and is dependent on the character of the powder; for example, it is possible that in some systems with a broad particle size range the initial stage may be essentially nonexistent.

Lastly, it is evident that the nature of the mass transport or diffusion path is not the same for the identified three stages of sintering. It is then unrealistic to attempt to develop a single equation based on basic principles to cover the entire sintering process that would be applicable to all systems. On the other hand, it is realistic to have mathematical expressions for the sintering kinetics that

apply to each stage of sintering with step one as the mass transport rate controlling step and another set with step two as the rate controlling step.

ACKNOWLEDGMENTS

This work was supported by the Division of Materials Sciences, Office of Basic Energy Sciences, U. S. Department of Energy.

REFERENCES

1.(a) Carl E. Hoge and Joseph A. Pask, "Thermodynamics of Solid State Sintering," in "Physics of Sintering, vol. 5," edited by M. M. Ristic, Boris Kidric Institute of Nuclear Sciences, Beograd, Yugoslavia, pp. 109-142, 1973.

1.(b) Carl E. Hoge and Joseph A. Pask, "Thermodynamics and Geometric Considerations of Solid State Sintering," Ceramurgia International, vol. 3, No. 3, pp. 95-99, July-September 1977.

2. Carl E. Hoge and Joseph A. Pask, "Thermodynamic Aspects of Solid State Sintering," in "Sintering and Catalysis, Materials Science Research, v. 10," edited by G. C. Kuczynski, Plenum Publishing Corp., New York, pp. 229-238, 1975.

3. Carl E. Hoge, Boon Wong and Joseph A. Pask, "Dependence of Sintering Characteristics on Thermodynamic and Geometric Factors," in "Ceramic Microstructures - '76," edited by Richard M. Fulrath and Joseph A. Pask, Westview Press, Boulder, Colorado, pp. 246-254, 1977.

4. Boon Wong and Joseph A. Pask, "Experimental Analysis of Sintering of MgO Compacts," to be published.

FIGURE CAPTIONS

1. Schematic of a two sphere model showing shrinkage:
   (a) Mass transport from grain boundary region to neck region is slow step, and (b) from neck region into free surface region is slow step.
2. Cross-section through neck region in the early stages of sintering when reverse curvature exists. Text describes vacancy and mass transport paths.
3. Sintering of a 3 sphere pore. Pore closes and dihedral angle increases to 60° as sphere centers move toward each other.
4. Shrinkage along (100), (111) and (110) planes in fcc packing of spheres.
5. Sintering of a planar pore formed by four spheres. Pore closes as dihedral angle approaches 90°.
6. Shrinkage along (100) and (110) planes in sc packing of spheres.
7. Planar packing of spheres with a coordination of three. Greater interpenetration at grain boundaries is necessary to achieve densification in the plane.
8. Effect of fcc, sc and dc packings of uniform size spheres on decrease of porosity vs. time curves.
9. Effect of sphere size in compacts with sc packing on densification rates.
10. Close packed plane in fcc packing with pore on triple point and one grain absent.
11. A large pore with many coordinating grains in an alumina compact. It was formed by adding large organic spheres to alumina powder

which were oxidized on heating.

12. Schematic examples of factors causing grain boundary motions in sintering compacts.

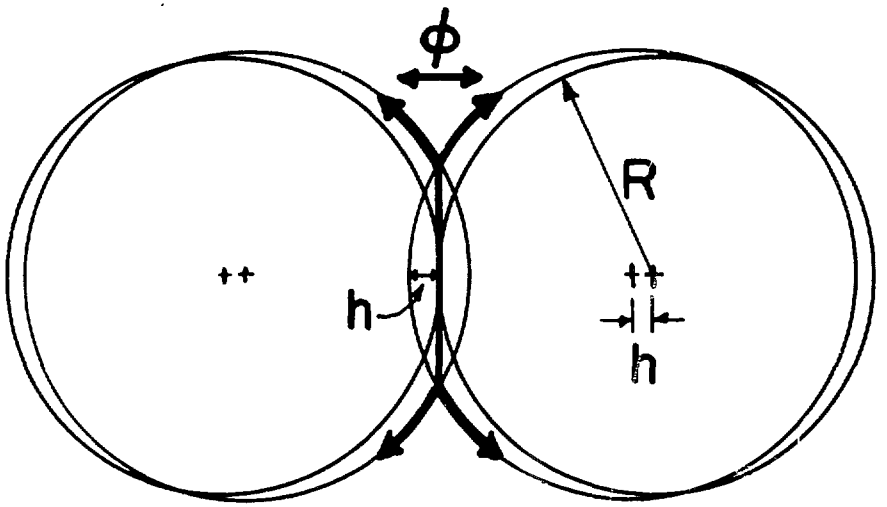

$$dG = \gamma_{SV}\, dA_{SV} + \gamma_{GB}\, dA_{GB}$$

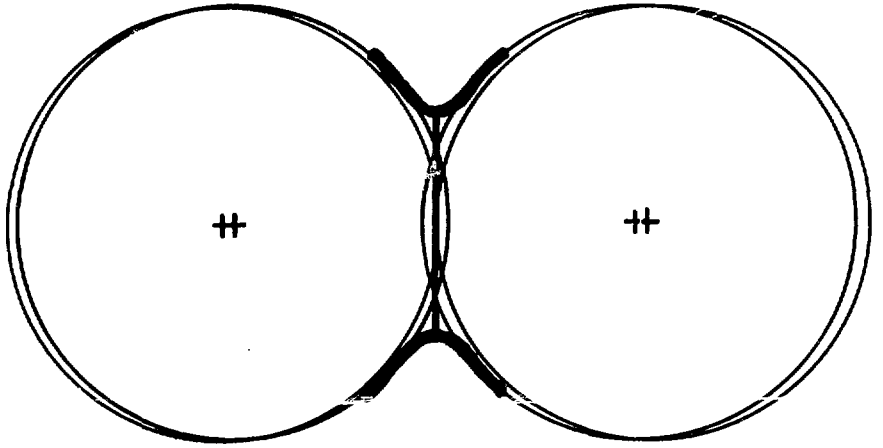

$$\gamma_{GB} = 2\gamma_{SV} \cos \phi/2$$

XBL 789-5743

Fig. 1

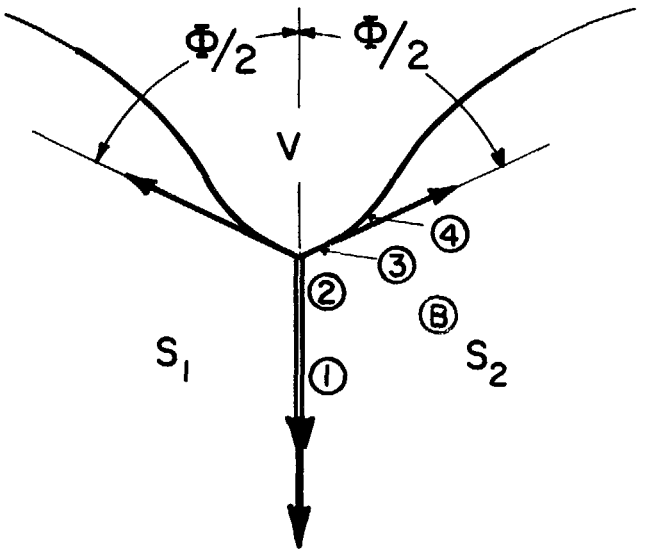

$$\gamma_{S_1S_2} < \gamma_{S_1V} \qquad \gamma_{S_2S_1} < \gamma_{S_2V}$$

$$\gamma_{GB} = \gamma_{S_1S_2} + \gamma_{S_2S_1}$$

$$\gamma_{GB} < \gamma_{S_1V} + \gamma_{S_2V}$$

$$\gamma_{GB} = \gamma_{S_1V} \cos \phi/2 + \gamma_{S_2V} \cos \phi/2$$

$$\gamma_{GB} = 2\gamma_{SV} \cos \phi/2$$

$$\gamma_{GB}/\gamma_{SV} = 2\cos \phi/2$$

At nonequilibrium

$$\mu_④ > \mu_③ > \mu_② > \mu_① \geq \mu_Ⓑ$$

XBL 789-5744

Fig. 2

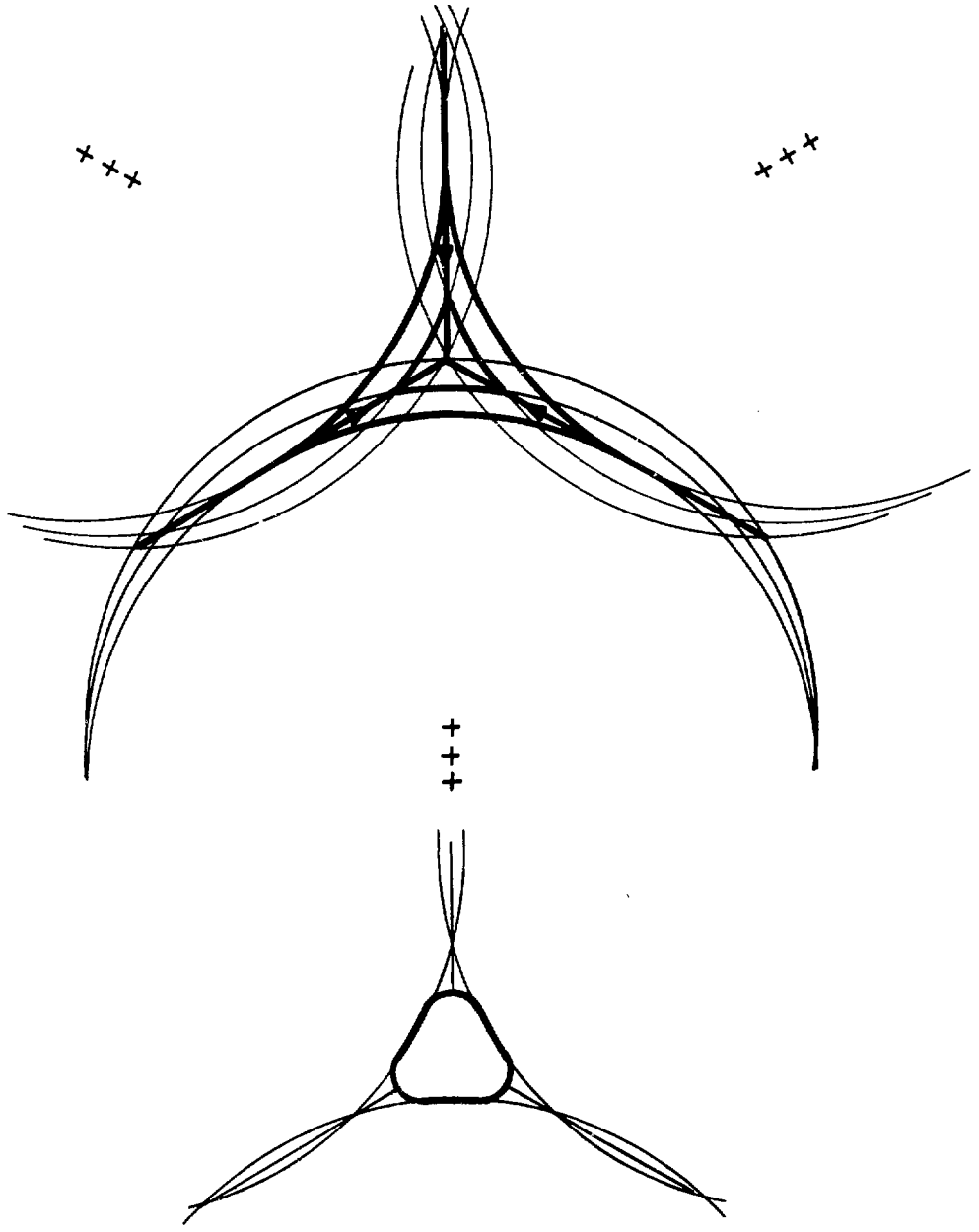

XBL 789-5750

Fig. 3

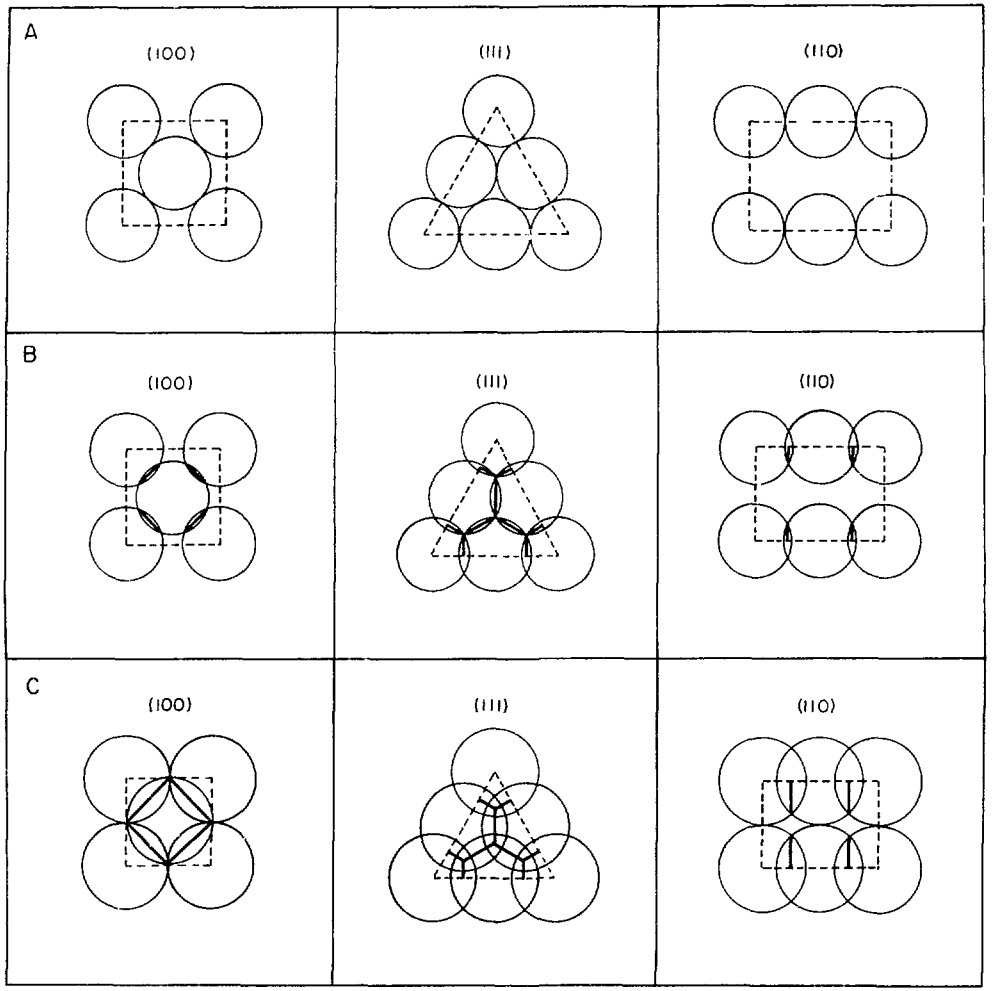

XBL 749-7294

Fig. 4

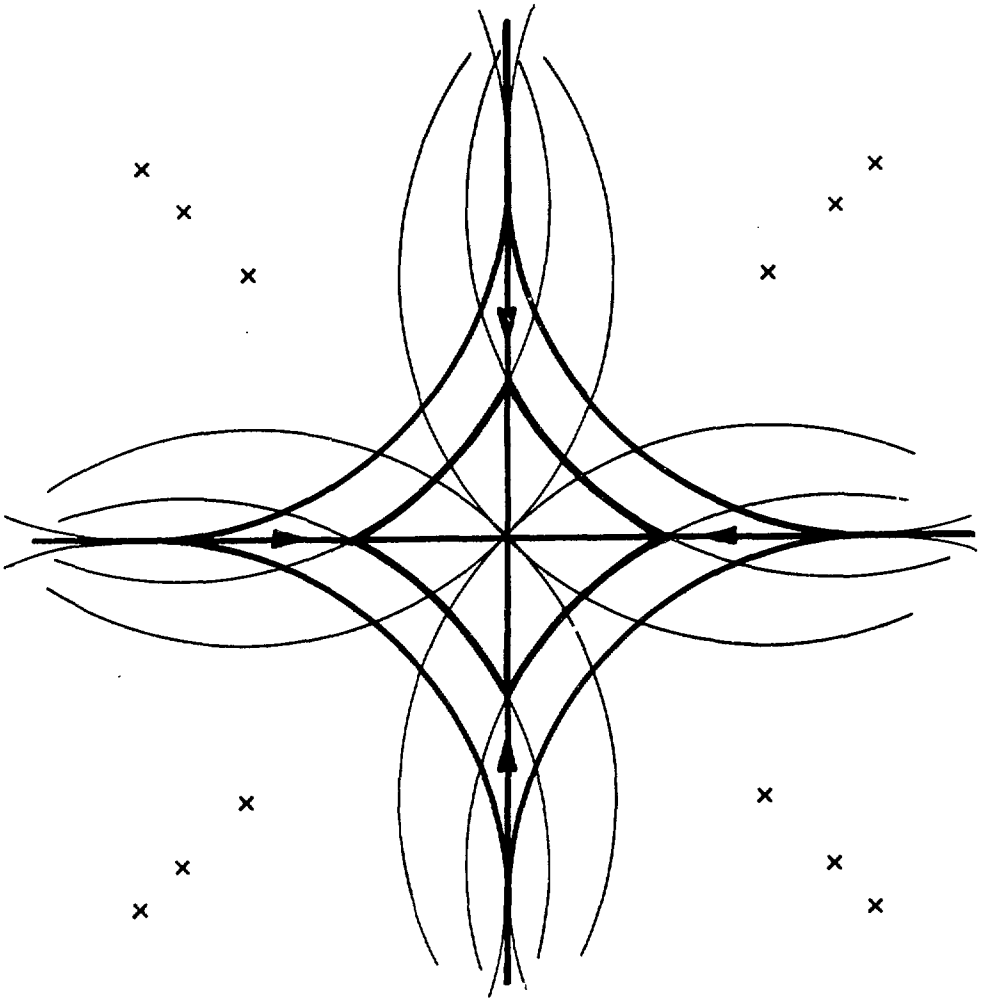

XBL 789-5752

Fig. 5

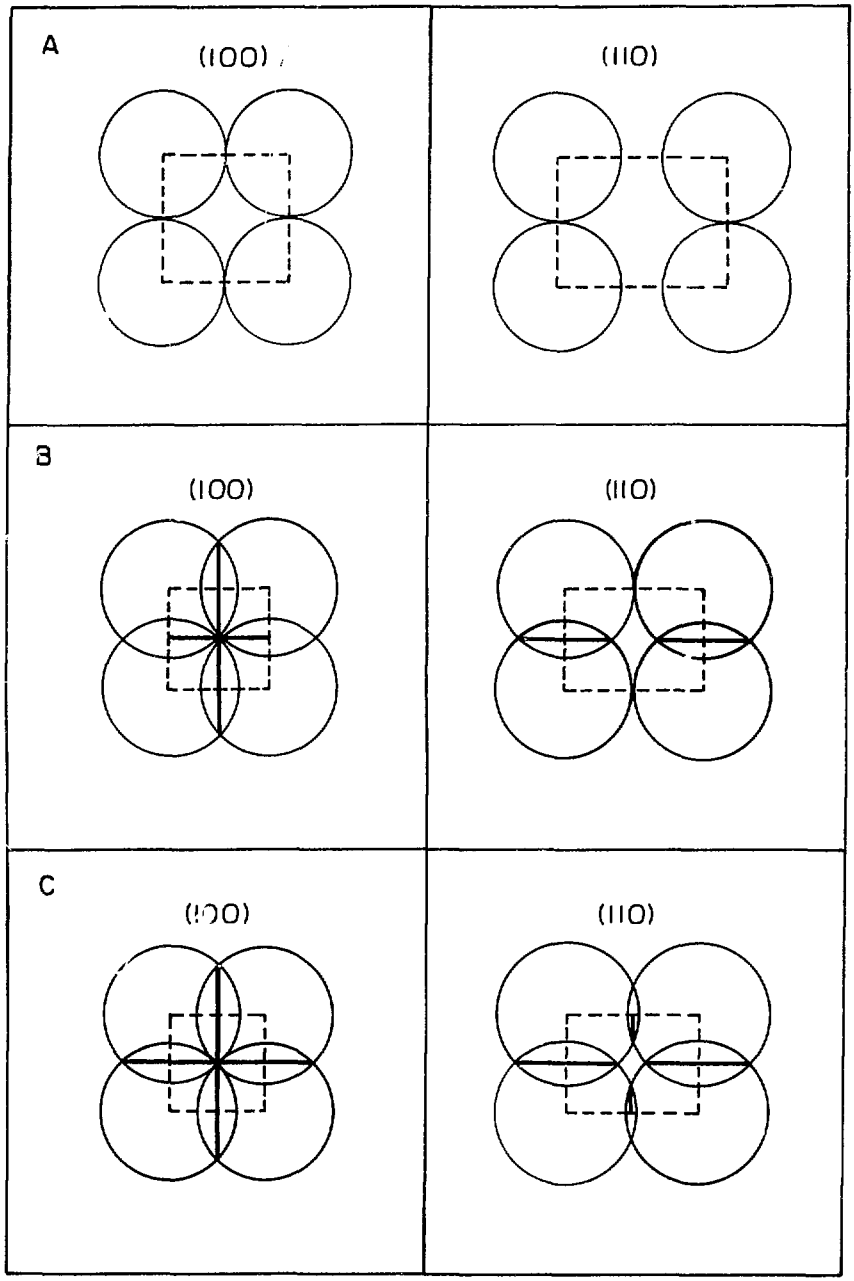

XBL 749-7293

Fig. 6

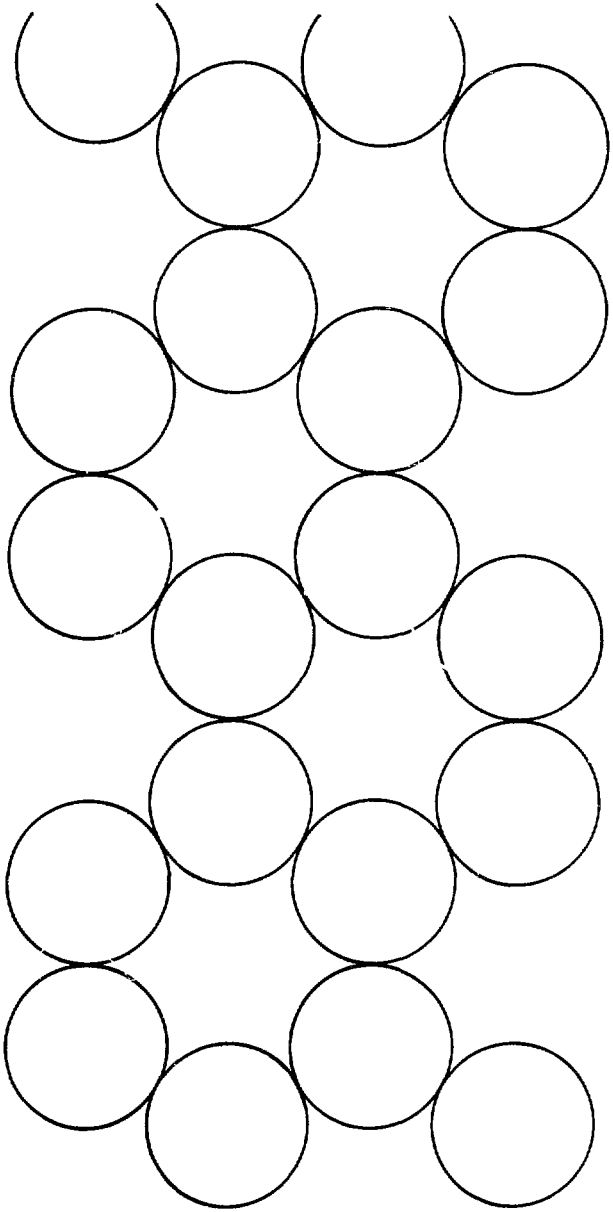

XBL 789-5751

Fig. 7

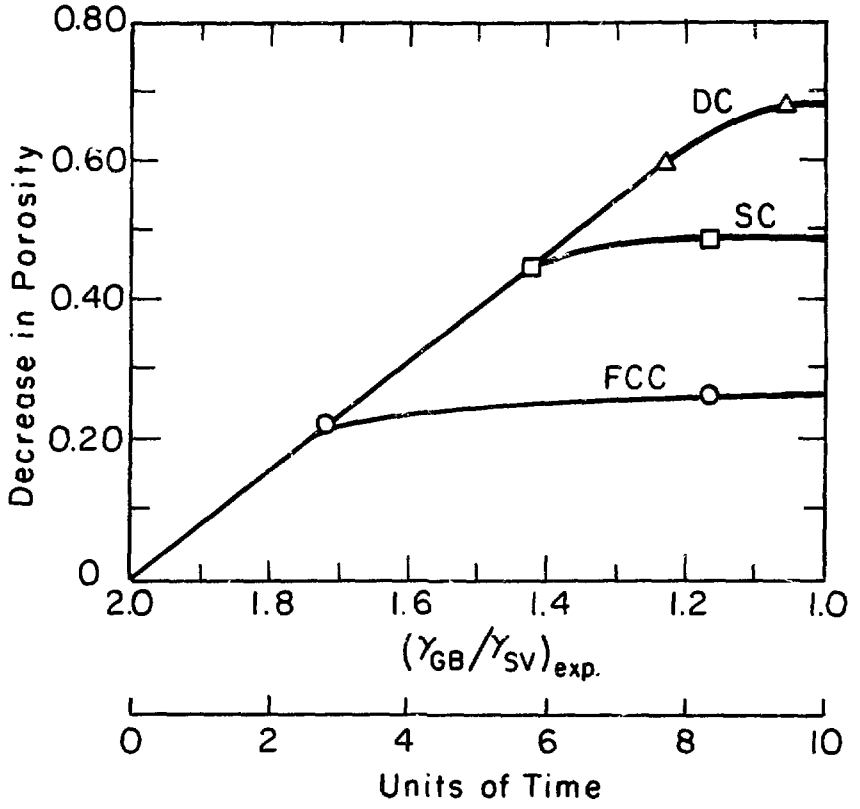

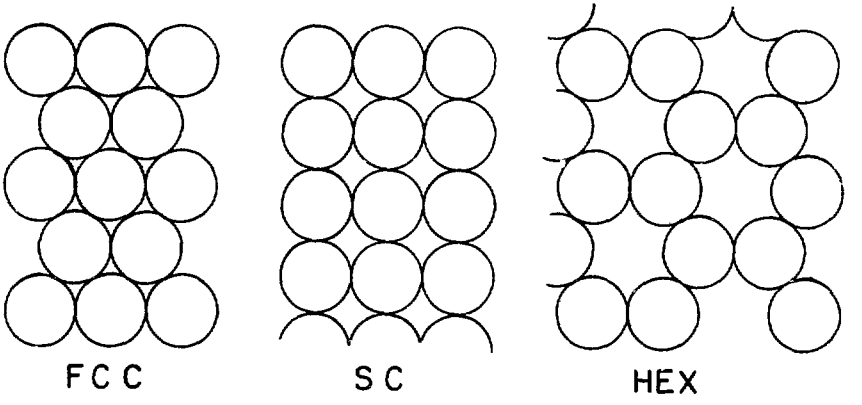

XBL 789-5749A

Fig. 8

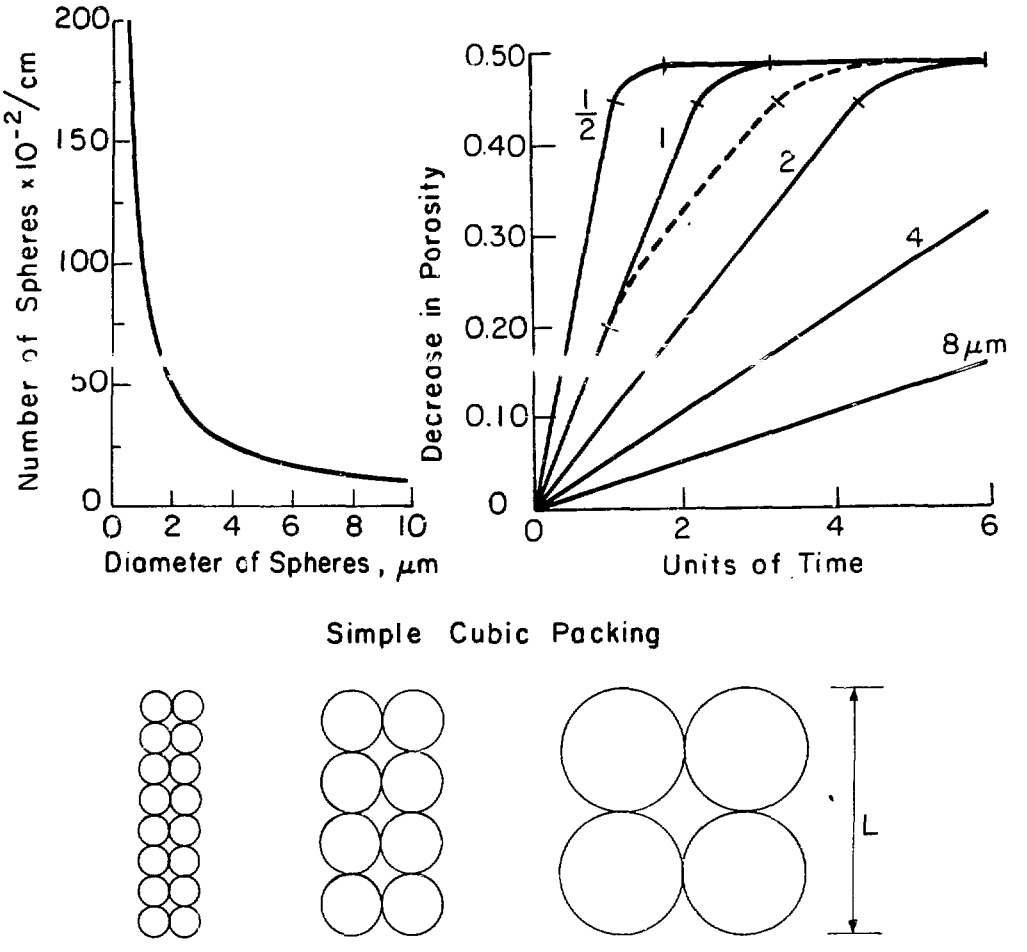

XBL 789-5748A

Fig. 9

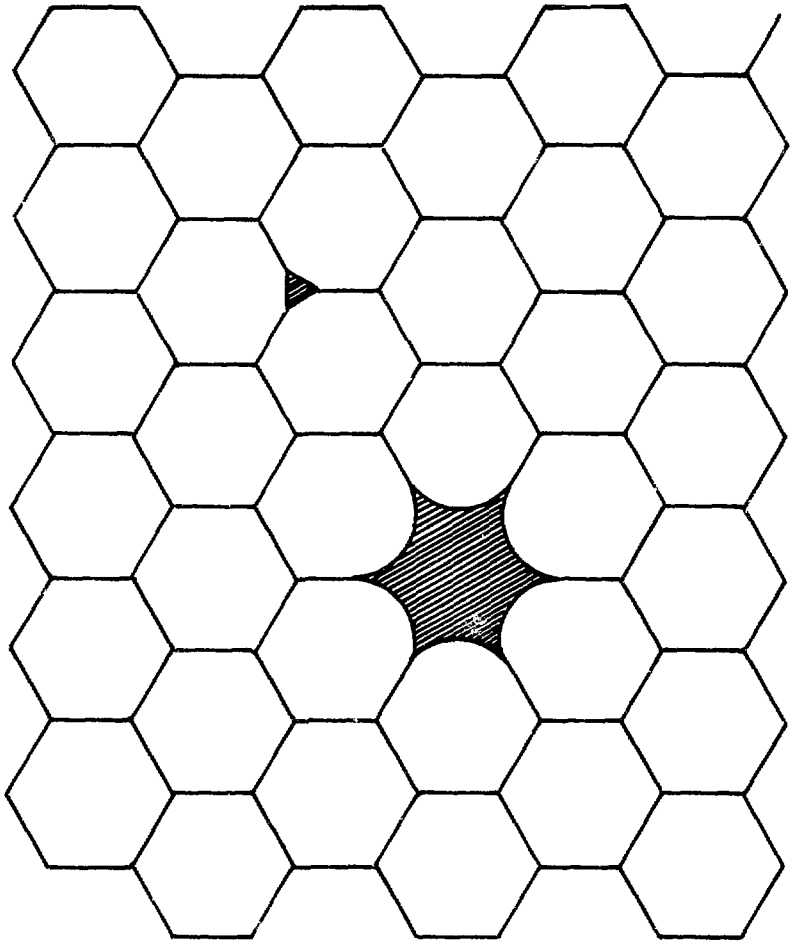

XBL 789-5747

Fig. 10

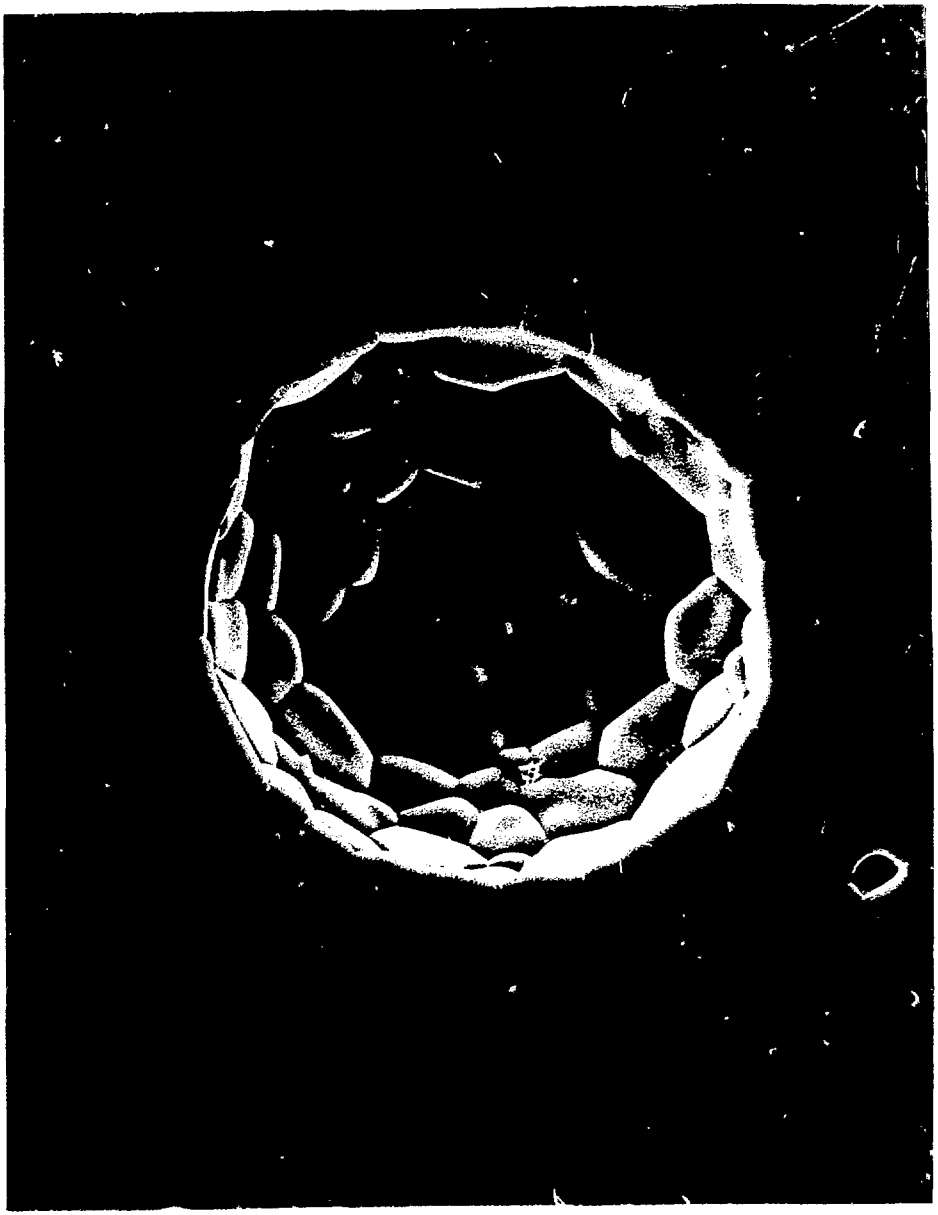

XBB786-7483

Fig. 11

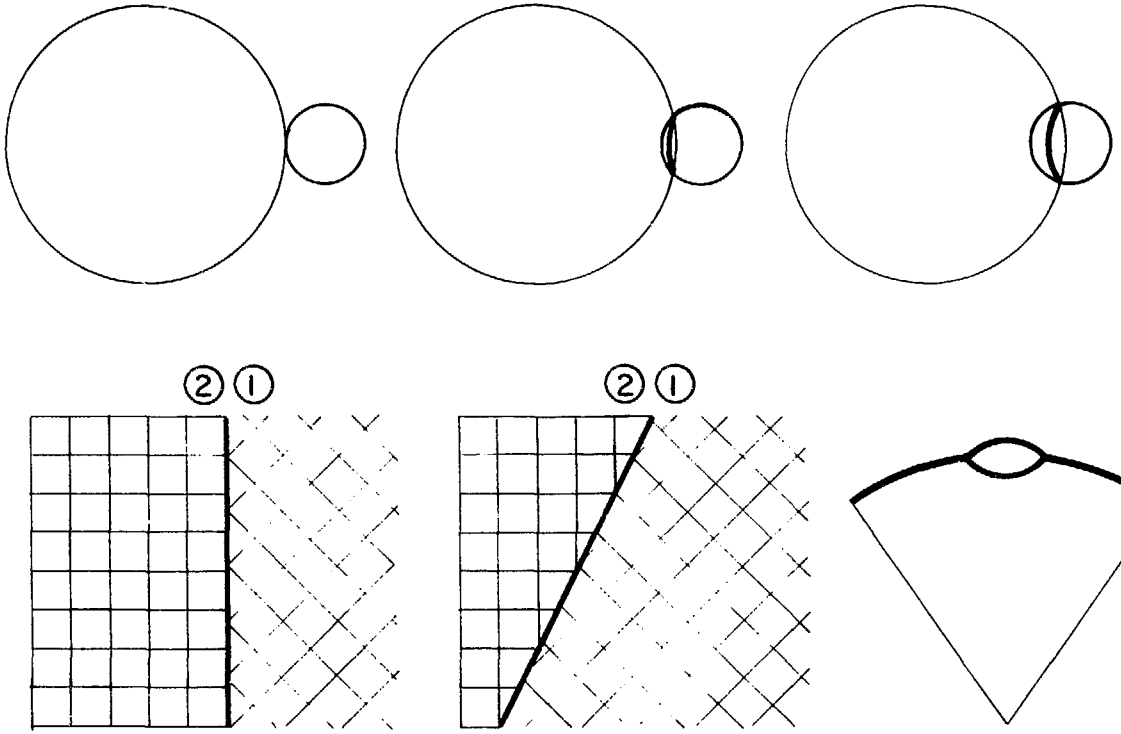

XBL 789-5746

Fig. 12